Contents

Figures
Supplementary Figure 1 | Flow cytometry gating strategy.
Supplementary Figure 2 | IPA and GSEA of electromechanically matured cardiac tissues.
Supplementary Figure 3 | Cardiac Gene Set Enrichment for Gene Ontology Biological Processes in matured human cardiac tissues.
Supplementary Figure 4 | Cardiac pathway enrichment and drug responses within matured human cardiac tissues.
Supplementary Figure 5 | Proteomic analysis maintains biological fidelity of tissues when cultured in *Multi-organ* tissue chip.
Supplementary Figure 6 | Schematic details models developed for simulation of studies without an endothelial barrier, endothelial barrier details, and mass balance for drugs over time.
Supplementary Figure 7 | FITC-dextran (3 kDa) diffusion and binding to the tissue chip.
Supplementary Figure 8 | Doxorubicin metabolism within the engineered liver tissue.
Supplementary Figure 9 | Experimental data and PK model of doxorubicin treatment in the *Mixed* tissue chip.
Supplementary Figure 10 | *In vitro* biomarkers of doxorubicin cardiotoxicity in multi-tissue chips.
Supplementary Figure 11 | *In vitro* biomarkers of doxorubicin cardiomyopathy in isolated tissue chips.
Supplementary Figure 12 | *In vitro* biomarkers of doxorubicin cardiomyopathy in perfusate of multi-tissue chips.

Tables
Supplementary Table 1 | Tissue specifications.
Supplementary Table 2 | Media compositions for each tissue type.
Supplementary Table 3 | Modeling parameters.
Supplementary Table 4 | Terms used in the computational model and their meaning.

Videos
Supplementary Video 1 | Assembly of the tissue chip.

References

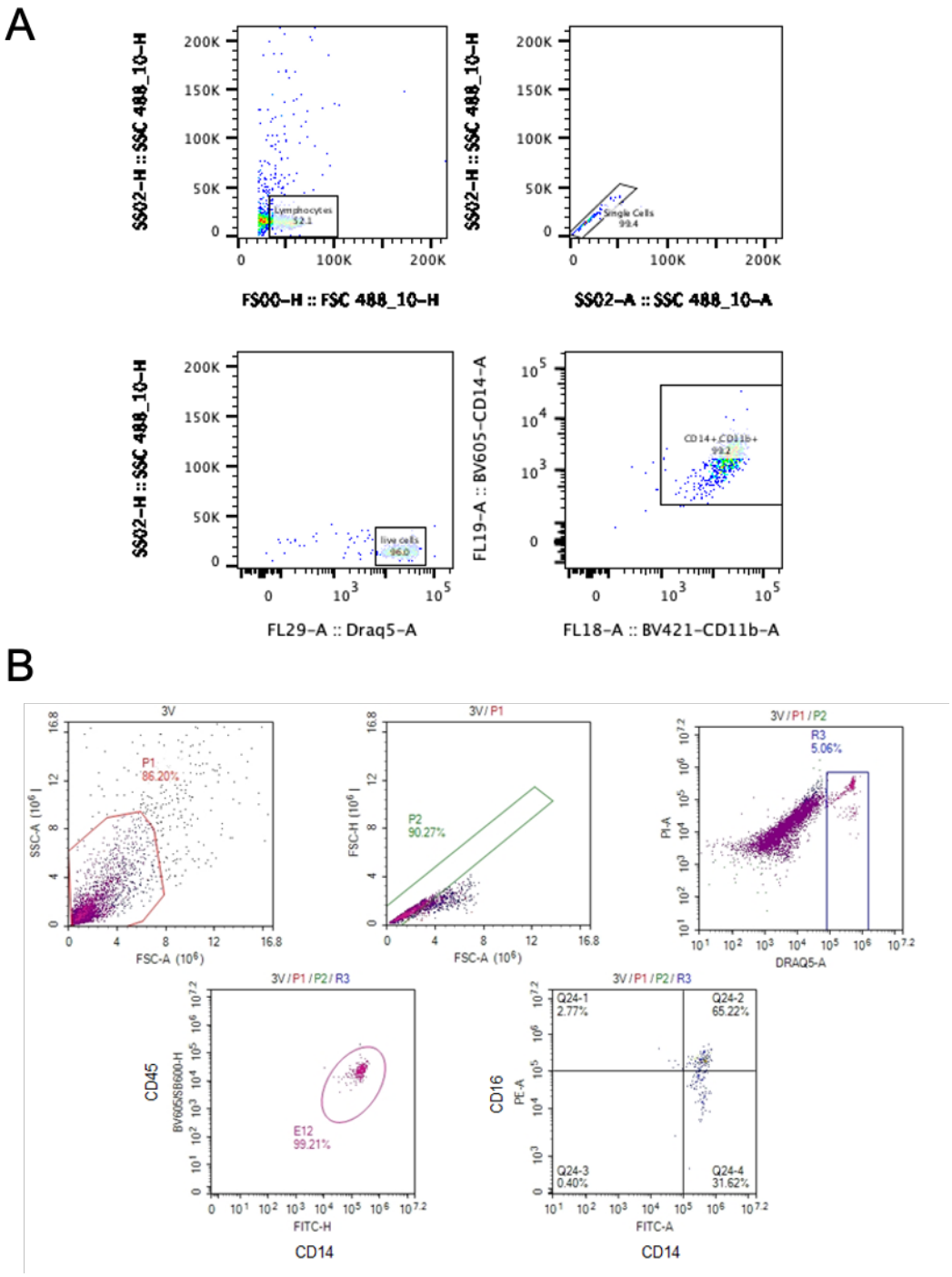

Supplementary Figure 1 | Flow cytometry gating strategy. a, Example gating strategy for magnetic-sorted CD14⁺ monocytes from human peripheral blood, acquired on Bio-Rad ZE5 Cell Analyzer. **b,** Example gating strategy for circulating cells isolated from the *Multi-organ* tissue chips, acquired on Agilent NovoCyte Quanteon.

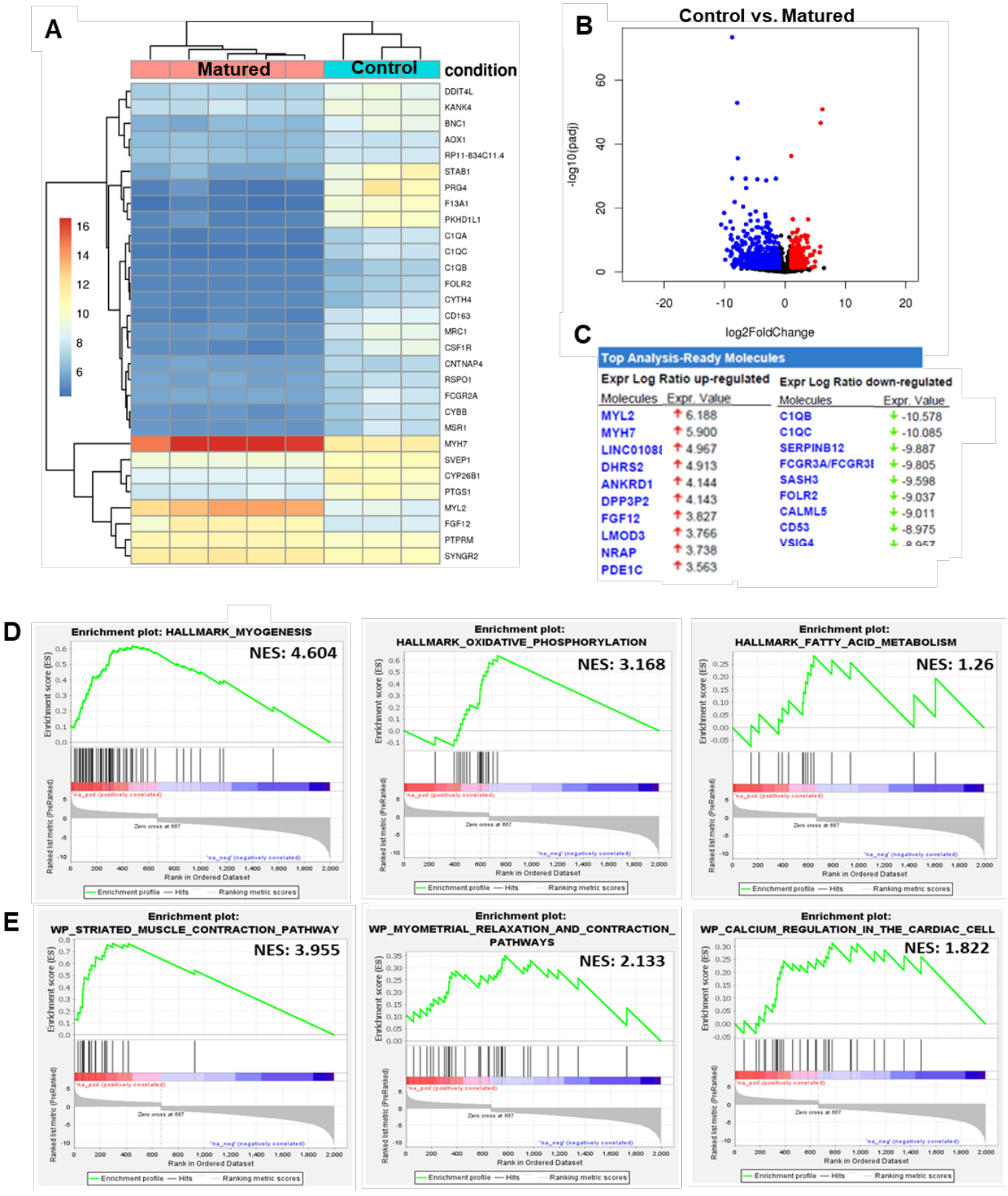

Supplementary Figure 2 | IPA and GSEA of electromechanically matured cardiac tissues. a, RNA sequencing heatmap of control heart tissues versus electromechanically matured tissues. **b,** Volcano plot of control versus matured cardiac tissue gene expression. **c,** Top Analysis Ready Molecules as determined by IPA Analysis. **d-e,** Gene Set Enrichment of Hallmark Pathways (**d**) and WikiPathways (**e**) for matured versus control heart tissues.

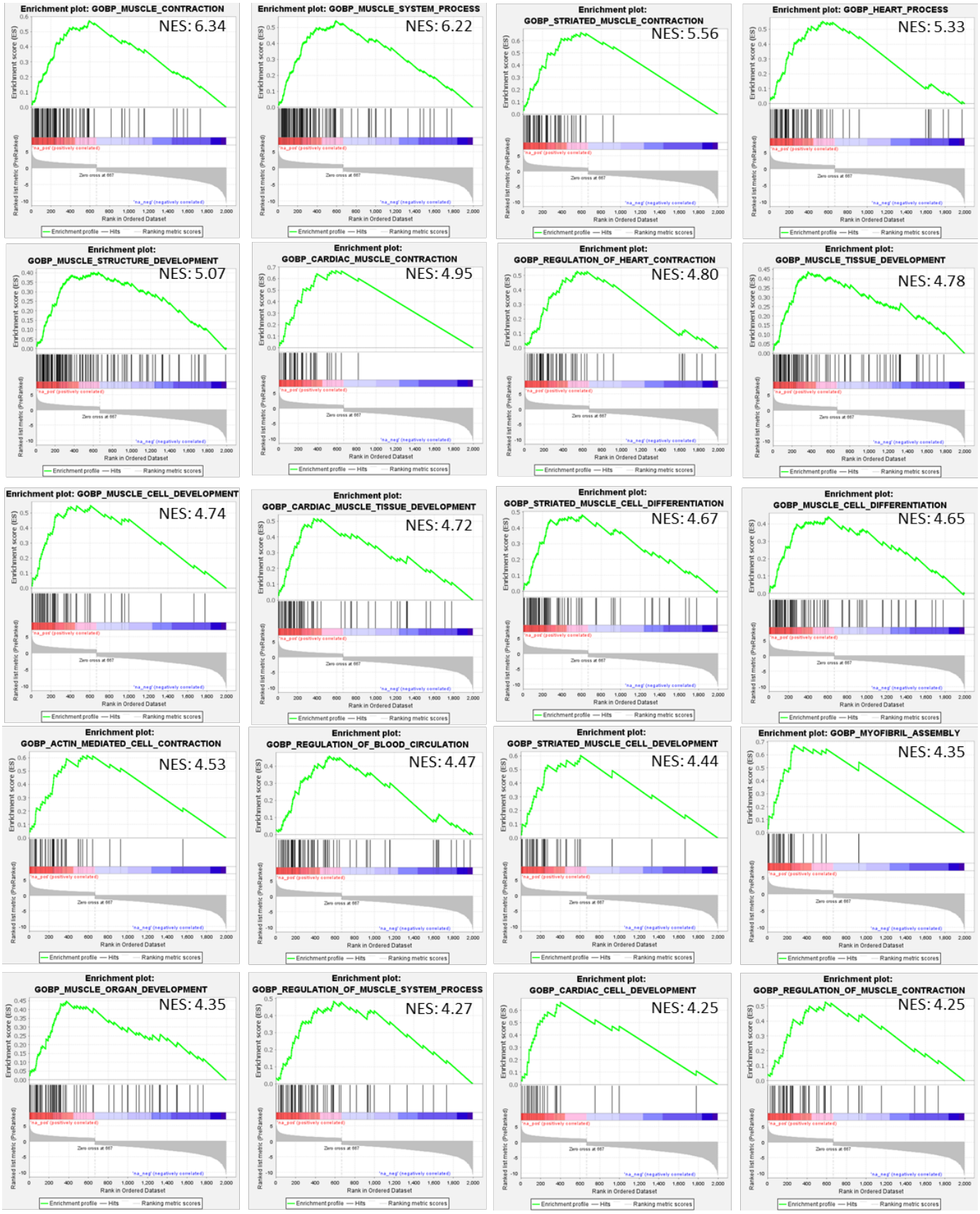

Supplementary Figure 3 | Cardiac Gene Set Enrichment for Gene Ontology Biological Processes in matured human cardiac tissues. Gene Set Enrichment Plots of the enriched Gene Ontology Biological Processes for matured versus control heart tissues.

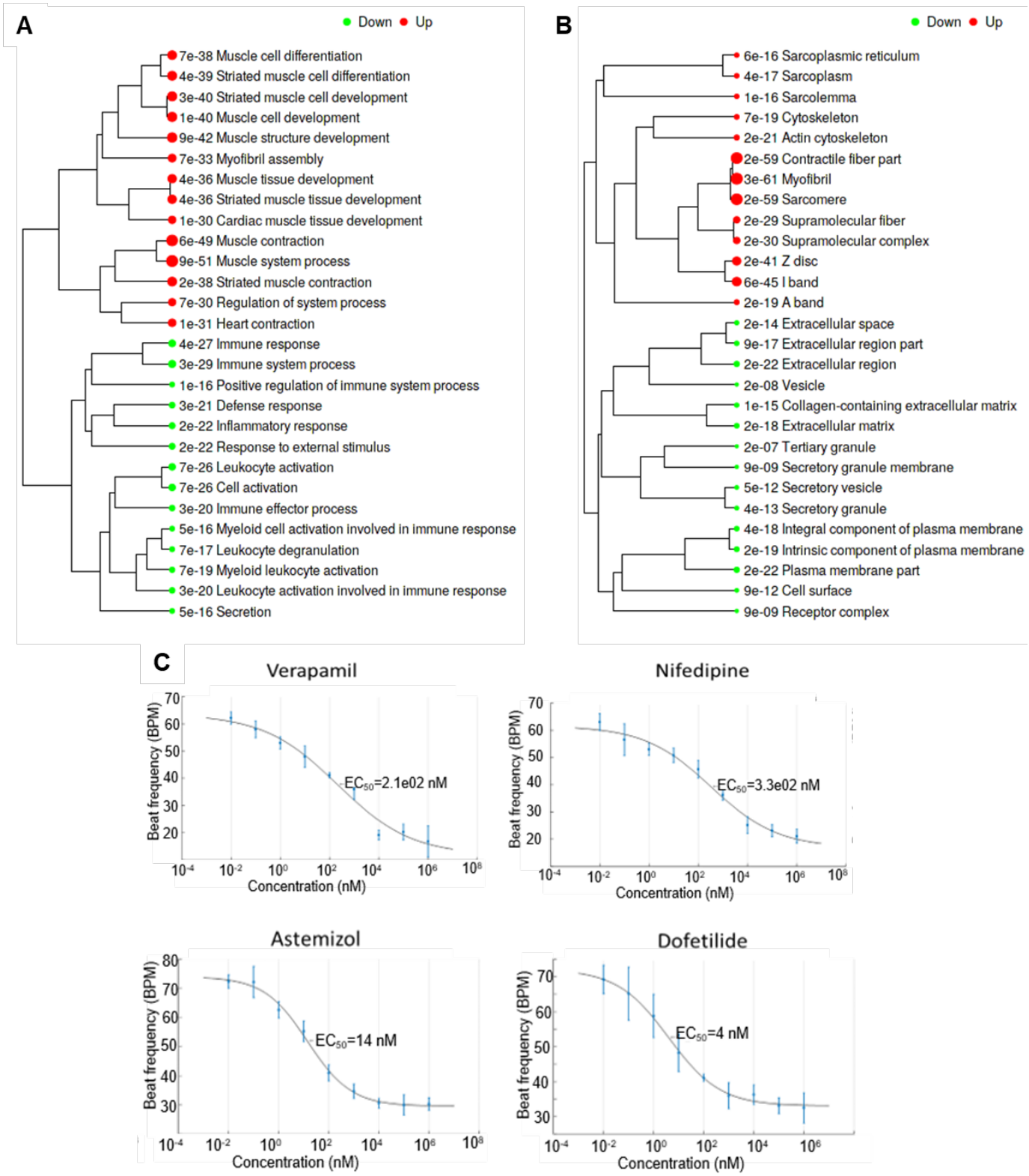

Supplementary Figure 4 | Cardiac pathway enrichment and drug responses within matured human cardiac tissues. a-b, Gene Ontology of Biological Processes (**a**) and Cellular components (**b**) for electromechanically matured versus control heart tissues, using RNA sequencing analysis between control heart tissues versus electromechanically matured tissues. **c,** Mature tissues were further validated by measuring dose-dependent responses (n=3-6, shown as mean with 95% confidence interval) to calcium signaling drugs, using calcium channel blockers.

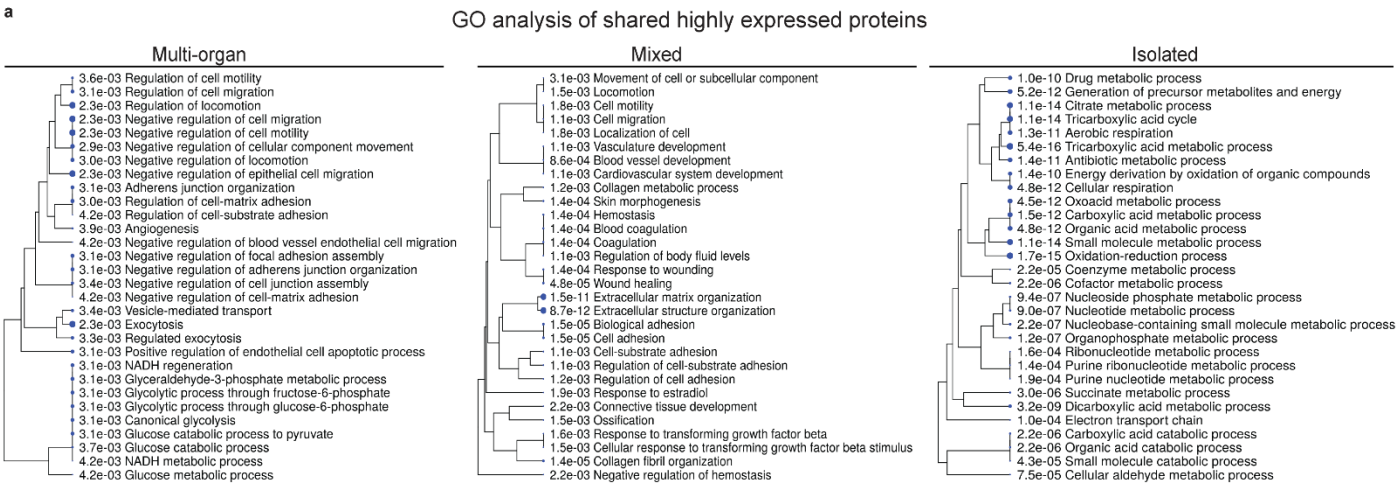

Supplementary Figure 5 | Proteomic analysis maintains biological fidelity of tissues when cultured in *Multi-organ* tissue chip. a, Comparison of shared highly expressed proteins (present within all engineered organs within each experimental group) using Gene Ontology (GO) analysis identifies shared gene pathways that are highly expressed amongst all the different engineered organs when cultured in each linked tissue chip configuration.

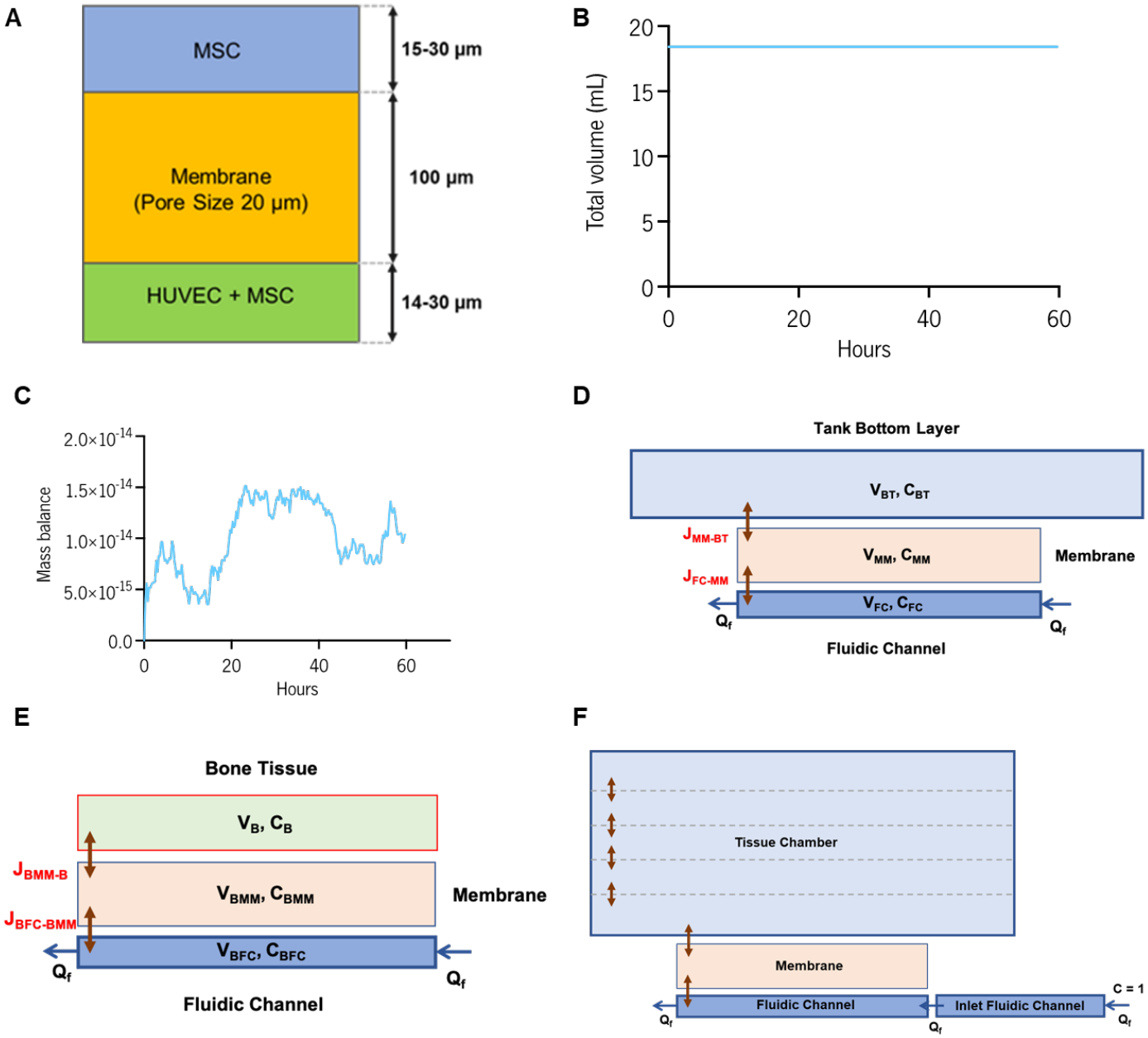

Supplementary Figure 6 | Schematic details models developed for simulation of studies without an endothelial barrier, endothelial barrier details, and mass balance for drugs over time. a, Detailed schematic of the endothelial barrier. **b-c,** Volume (**b**) and mass (**c**) conservation for doxorubicin from the reservoir over time. **d,** Bottom layer of the tissue chambers of liver, heart, and skin. **e,** Bottom layer of the bone tissue chamber. **f,** Five discretization test case model for doxorubicin.

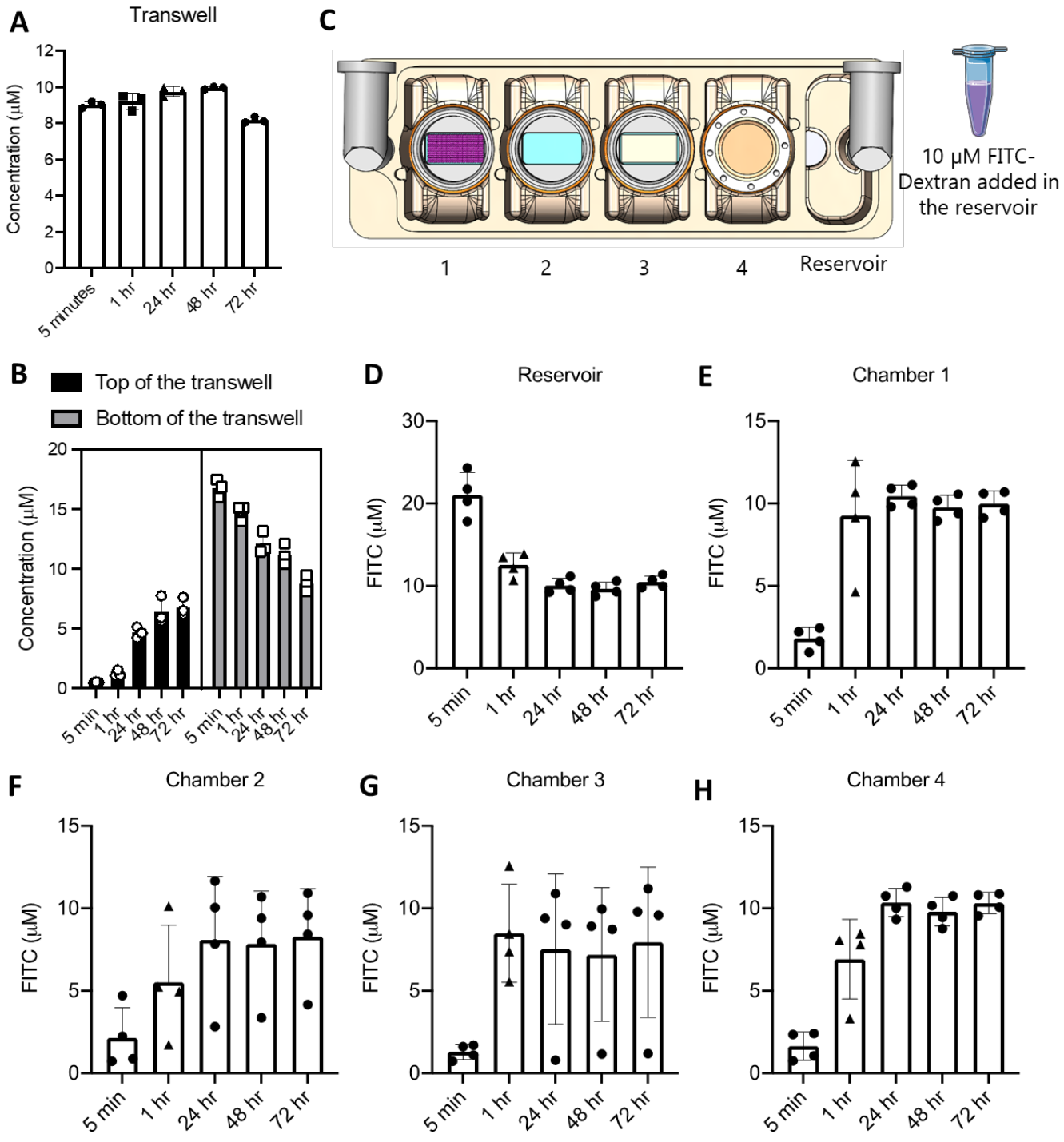

Supplementary Figure 7 | FITC-dextran (3 kDa) diffusion and binding to the tissue chip. a, Absorption (n=3 biological replicates). **b,** Diffusion through transwell (n=3 biological replicates). **c,** Schematic of the experimental design to evaluate FITC-Dextran diffusion in the chip over time. **d-h,** Experimental results of FITC-Dextran diffusion in the tissue chip for the reservoir (**d**), chamber 1 (**e**), chamber 2 (**f**), chamber 3 (**g**), and chamber 4 (**h**) over time (n=4 biological replicates). Data are mean ± SD.

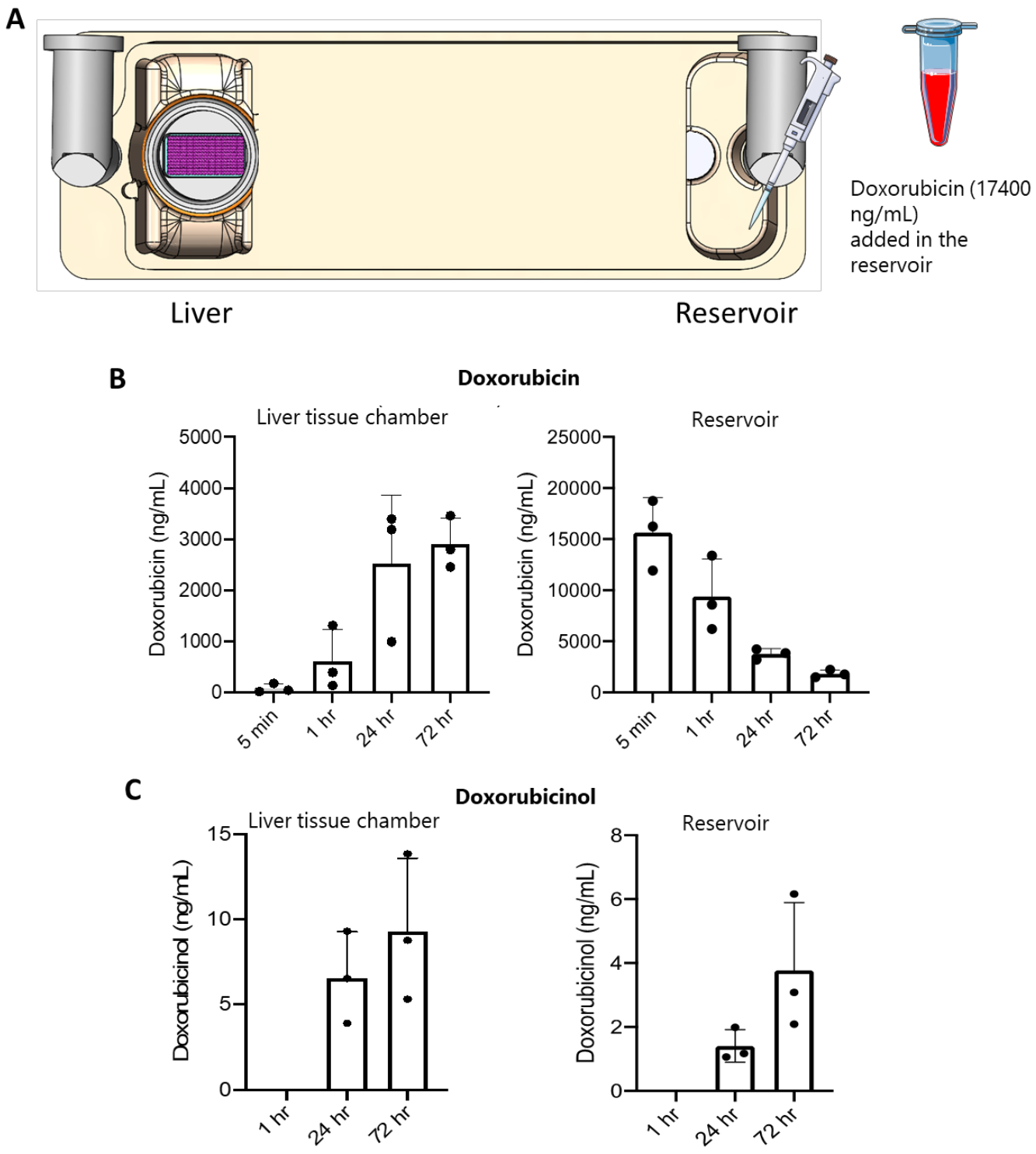

Supplementary Figure 8 | Doxorubicin metabolism within the engineered liver tissue. a, Schematic of the experimental design. **b-c,** Doxorubicin (**b**) and doxorubicinol (**c**) levels in the liver tissue chamber and in the reservoir measured over time, as measured by UPLC-MSMS. Data are mean ± SD (n=3 biological replicates).

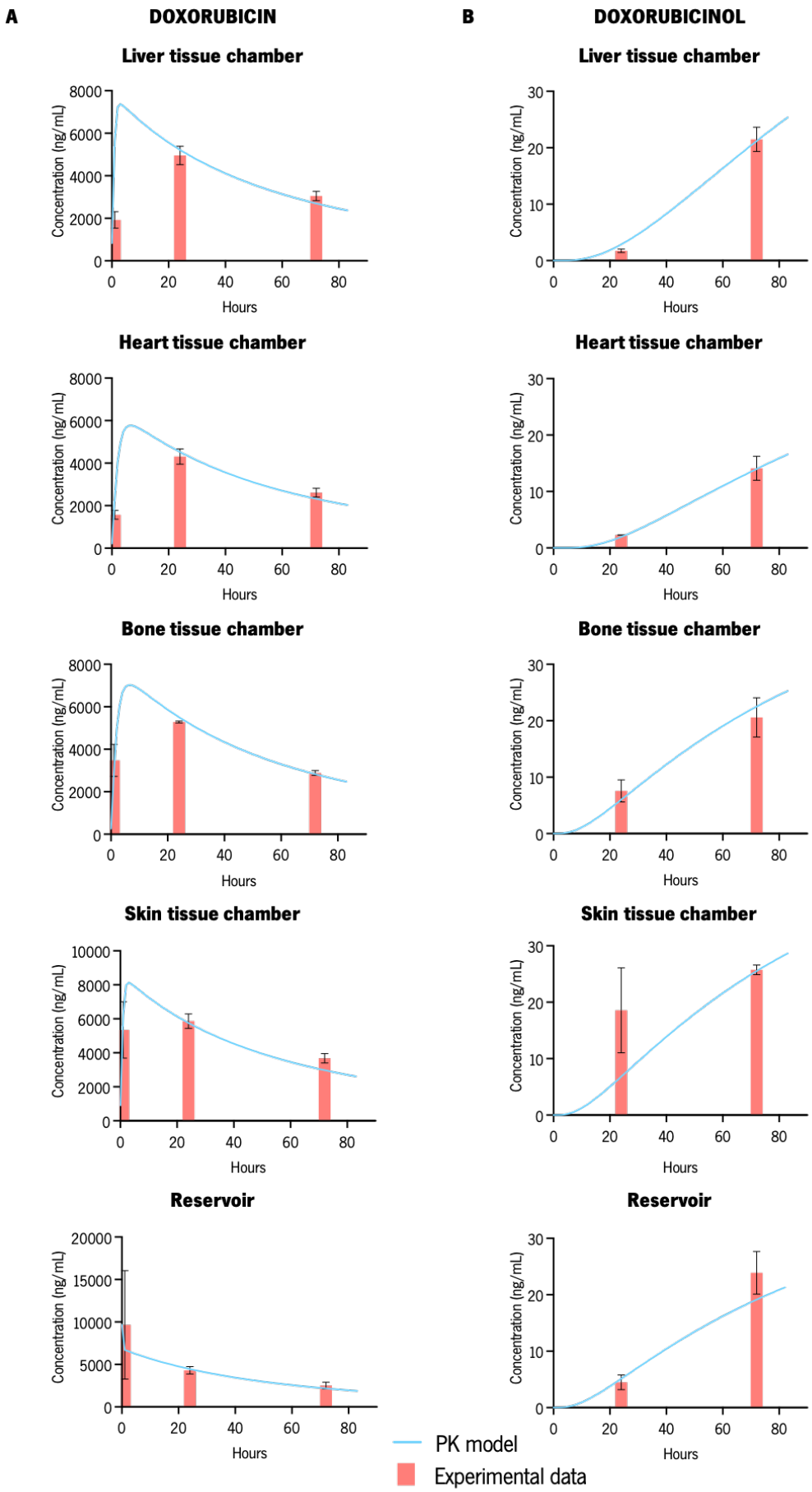

Supplementary Figure 9 | Experimental data and PK model of doxorubicin treatment in the *Mixed* tissue chip. a-b, Doxorubicin (**a**) and doxorubicinol (**b**) levels, measured over time by UPLC-MSMS within all tissue chambers and in the reservoir (red bar), compared with prediction of the computational PK model (blue line). Data are mean ± SD.

A

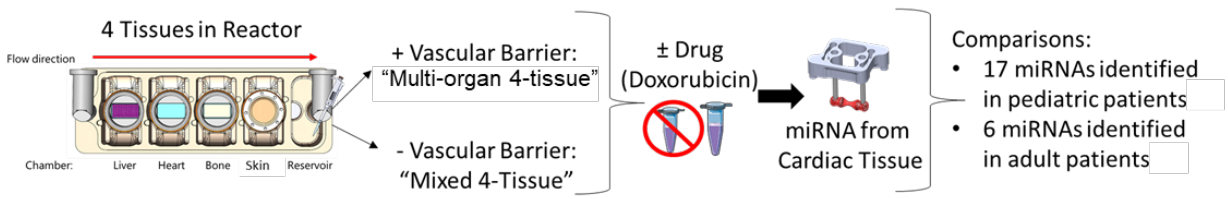

miRNA Biomarkers of Doxorubicin Induced Cardiomyopathy – Pediatric Clinical Trial[17] Comparison

B

Multi-organ 4-tissue Cardiac Tissue miRNA (Doxorubicin vs Control)

miRNA	GSEA plot	NES	FC	pval
hsa-miR-143-3p		-0.89	-1.01*	2.70e-03
hsa-miR-199a-5p		-2.66	-3.13*	4.10e-05
hsa-miR-107-5p		-0.93	-1.04*	2.90e-03
hsa-miR-320a		1.12	1.43*	7.30e-03
hsa-miR-103a-3p		-1.09	-1.11*	2.70e-03
hsa-miR-145-5p		-1.19	-1.22*	3.30e-03
hsa-miR-181a-5p		-1.19	-1.22*	3.90e-03
hsa-miR-100-5p		-1.29	-1.41*	4.20e-03
hsa-miR-499a-5p		-9.98	-10.01	1.20e-08
hsa-miR-146a-5p		-3.23	-3.45*	9.80e-06
hsa-miR-210-3p		-2.09	-2.11	9.10e-04
hsa-miR-92a-3p		-1.76	-1.8	1.80e-04
hsa-miR-342-3p		-1.02	-1.03*	1.10e-03
hsa-miR-142-3p		1.52	1.61	3.10e-03
hsa-miR-150-5p		1.56	1.63	3.20e-03
hsa-miR-29c-3p		-0.97	-1.23	1.10e-03
hsa-miR-486-5p		-2.38	-2.45	1.60e-04

0 750 1500 2250 3000

C

Mixed 4-tissue Cardiac Tissue miRNA (Doxorubicin vs Control)

miRNA	GSEA plot	NES	FC	pval
hsa-miR-143-3p		1.89	1.98	1.80e-03
hsa-miR-199a-5p		-14.26	-14.03	4.10e-17
hsa-miR-107-5p		1.21	1.34	9.20e-03
hsa-miR-320a		-2.01	-2.07	1.90e-03
hsa-miR-103a-3p		1.19	1.21	3.70e-03
hsa-miR-145-5p		3.23	3.45	1.30e-05
hsa-miR-181a-5p		0.59	0.72	1.10e-02
hsa-miR-100-5p		-2.13	-2.41*	1.20e-04
hsa-miR-499a-5p		1.78	1.91*	2.30e-03
hsa-miR-146a-5p		-1.23	-1.45*	9.80e-04
hsa-miR-210-3p		-3.19	-3.21	1. 1e-05
hsa-miR-92a-3p		-1.56	-1.6	7.80e-03
hsa-miR-342-3p		1.12	1.13	1.10e-03
hsa-miR-142-3p		-1.22	-1.25*	3.10e-03
hsa-miR-150-5p		1.26	1.33	5.20e-03
hsa-miR-29c-3p		1.17	1.19*	2.10e-03
hsa-miR-486-5p		-1.38	-1.45	6.50e-03

0 750 1500 2250 3000

miRNA Biomarkers of Doxorubicin Induced Cardiomyopathy – Adult Clinical Trial[20] Comparison

D

Multi-organ 4-tissue Cardiac Tissue miRNA (Doxorubicin vs Control)

miRNA	GSEA plot	NES	FC	pval
hsa-miR-4638-3p		1.22	1.44	2.70e-03
hsa-miR-5096		1.66	3.23	4.30e-05
hsa-miR-4763-5p		-1.73	-1.84	3.30e-03
hsa-miR-1273g-3p		-1.28	-1.33	2.80e-03
hsa-miR-4726-5p		1.39	1.41	2.80e-03
hsa-miR-1273a		-43.2	-45.23	3.30e-19

0 750 1500 2250 3000

E

Mixed 4-tissue Cardiac Tissue miRNA (Doxorubicin vs Control)

miRNA	GSEA plot	NES	FC	pval
hsa-miR-4638-3p		-1.29	-1.38	2.80e-03
hsa-miR-5096		1.26	1.33	2.90e-03
hsa-miR-4763-5p		1.21	1.34	2.20e-03
hsa-miR-1273g-3p		1.92	1.93	4.90e-03
hsa-miR-4726-5p		-1.29	-1.31	2.70e-03
hsa-miR-1273a		1.23	1.45	2.30e-03

0 750 1500 2250 3000

Supplementary Figure 10 | *In vitro* biomarkers of doxorubicin cardiotoxicity in multi-tissue chips. a, Schematic detailing workflow characterizing miRNA expression between 4-tissue *Multi-organ* and *Mixed* tissue chips after doxorubicin treatment. **b-c,** Gene set enrichment analysis (GSEA) of miRNAs from four tissue *Multi-organ* (**b**) and *Mixed* (**c**) tissue chips after doxorubicin treatment as benchmarked against clinically identified biomarkers of doxorubicin toxicity in a pediatric study (Oatmen et al., 2018). **d-e,** Gene set enrichment analysis (GSEA) of miRNAs from four tissue *Multi-organ* (**d**) and *Mixed* (**e**) tissue chips after doxorubicin treatment as benchmarked against clinically identified biomarkers of doxorubicin toxicity in an adult study (Yadi et al., 2020). (*Consistent with clinical finding; Color codes – Blue (Negative Fold-Change), Red (Positive Fold-Change))

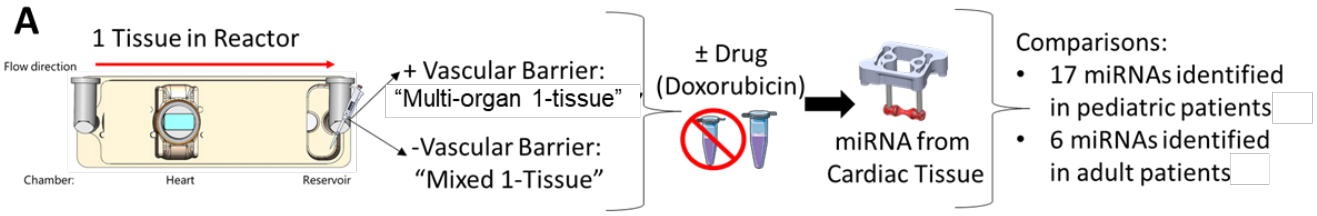

miRNA Biomarkers of Doxorubicin Induced Cardiomyopathy – Pediatric Clinical Trial[17] Comparison

B

Multi-organ 1-tissue Cardiac Tissue miRNA (Doxorubicin vs Control)

miRNA	GSEA plot	NES	FC	pval
hsa-miR-143-3p		-1.09	-1.18*	8.20e-03
hsa-miR-199a-5p		-1.16	-1.23*	9.10e-03
hsa-miR-107-5p		-1.2	-1.33*	9.50e-03
hsa-miR-320a		-1.15	-1.17	7.30e-03
hsa-miR-103a-3p		-1.12	-1.15*	6.70e-03
hsa-miR-145-5p		-1.23	-1.29*	1. 1e-03
hsa-miR-181a-5p		-1.59	-1.72*	1.30e-03
hsa-miR-100-5p		-1.33	-1.41*	1.10e-03
hsa-miR-499a-5p		1.58	1.71*	1.30e-03
hsa-miR-146a-5p		1.43	1.45	1.20e-03
hsa-miR-210-3p		-1.19	-1.21	9.80e-03
hsa-miR-92a-3p		-1.2	-1.23	9.90e-03
hsa-miR-342-3p		-1.22	-1.24*	1.10e-03
hsa-miR-142-3p		-1.32	-1.36*	1.10e-03
hsa-miR-150-5p		-1.56	-1.63*	1.30e-03
hsa-miR-29c-3p		1.27	1.29*	9.90e-02
hsa-miR-486-5p		-1.78	-1.95	1.60e-03

C

Mixed 1-tissue Cardiac Tissue miRNA (Doxorubicin vs Control)

miRNA	GSEA plot	NES	FC	pval
hsa-miR-143-3p		-2.82	-2.91*	1.90e-04
hsa-miR-199a-5p		18.02	19.21	1.20e-18
hsa-miR-107-5p		1.02	1.12	6.30e-03
hsa-miR-320a		1.12	1.22*	9.30e-03
hsa-miR-103a-3p		1.24	1.29	1.10e-02
hsa-miR-145-5p		-4.12	-4.23*	2.30e-06
hsa-miR-181a-5p		-1.24	-1.39*	1.30e-03
hsa-miR-100-5p		1.21	1.25	1.10e-02
hsa-miR-499a-5p		1.01	1.05*	9.50e-03
hsa-miR-146a-5p		1.31	1.35	1.10e-03
hsa-miR-210-3p		1.41	1.46*	1.30e-03
hsa-miR-92a-3p		1.11	1.15*	1.10e-02
hsa-miR-342-3p		1.21	1.25	1.10e-02
hsa-miR-142-3p		1.18	1.19	1.10e-02
hsa-miR-150-5p		-1.16	-1.17*	1.10e-02
hsa-miR-29c-3p		1.19	1.21*	1.10e-02
hsa-miR-486-5p		-1.26	-1.27	1.10e-02

miRNA Biomarkers of Doxorubicin Induced Cardiomyopathy – Adult Clinical Trial[20] Comparison

D

Multi-organ 1-tissue Cardiac Tissue miRNA (Doxorubicin vs Control)

miRNA	GSEA plot	NES	FC	pval
hsa-miR-4638-3p		-1.29	-1.38	2.20e-03
hsa-miR-5096		-1.26	-1.33	2.10e-03
hsa-miR-4763-5p		-1.3	-1.33	2.50e-03
hsa-miR-1273g-3p		-1.35	-1.37	2.30e-03
hsa-miR-4726-5p		-1.32	-1.35	2.70e-03
hsa-miR-1273a		-1.33	-1.39	1.10e-03

E

Mixed 1-tissue Cardiac Tissue miRNA (Doxorubicin vs Control)

miRNA	GSEA plot	NES	FC	pval
hsa-miR-4638-3p		-1.82	-1.91	2.90e-03
hsa-miR-5096		-1.02	-1.21	1.20e-03
hsa-miR-4763-5p		1.02	1.09	1.10e-03
hsa-miR-1273g-3p		1.12	1.19	1.90e-03
hsa-miR-4726-5p		-1.24	-1.29	2.50e-03
hsa-miR-1273a		-1.12	-1.23	2.30e-03

Supplementary Figure 11 | *In vitro* biomarkers of doxorubicin cardiomyopathy in isolated tissue chips. a, Schematic detailing workflow characterizing miRNA expression between 1-tissue *Multi-organ* and *Mixed* tissue chips after doxorubicin treatment. **b-c,** Gene set enrichment analysis (GSEA) of miRNAs from isolated tissue *Multi-organ* (**b**) and Mixed (**c**) chips after doxorubicin treatment as benchmarked against clinically identified biomarkers of doxorubicin toxicity in a pediatric study (Oatmen et al., 2018). **d-e,** Gene set enrichment analysis (GSEA) of miRNAs from isolated 1-tissue *Multi-organ* (**d**) and *Mixed* (**e**) tissue chips after doxorubicin treatment as benchmarked against clinically identified biomarkers of doxorubicin toxicity in an adult study (Yadi et al., 2020). (*Consistent with clinical finding; Color codes – Blue (Negative Fold-Change), Red (Positive Fold-Change))

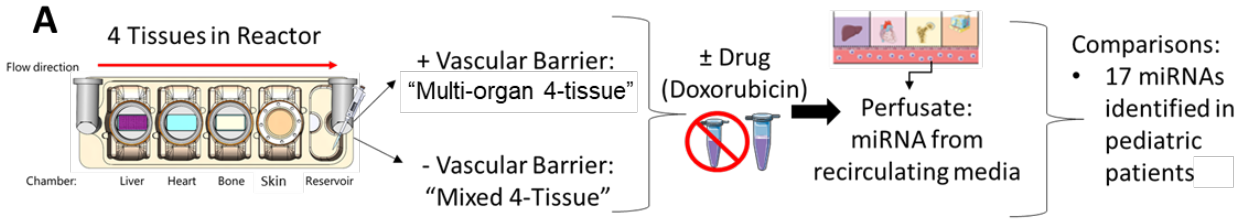

miRNA Biomarkers of Doxorubicin Induced Cardiomyopathy – Pediatric Clinical Trial[17] Comparison

B

Multi-organ 4-tissue Cardiac Tissue miRNA (Doxorubicin vs Control)				
miRNA	GSEA plot	NES	FC	pval
hsa-miR-143-3p		1.08	1.11	2.70e-03
hsa-miR-199a-5p		-2.23	-2.35*	1.50e-04
hsa-miR-107-5p		-1.09	-1.1*	2.70e-03
hsa-miR-320a		1.42	1.53*	3.10e-03
hsa-miR-103a-3p		1.07	1.1	2.70e-03
hsa-miR-145-5p		-1.21	-1.28*	2.90e-03
hsa-miR-181a-5p		1.09	1.12	2.70e-03
hsa-miR-100-5p		-1.25	-1.32*	2.73e-03
hsa-miR-499a-5p		-1.43	-1.53	3.10e-03
hsa-miR-146a-5p		-1.31	-1.41*	2.90e-03
hsa-miR-210-3p		-1.33	-1.41	2.90e-03
hsa-miR-92a-3p		1.34	1.42*	2.90e-03
hsa-miR-342-3p		1.19	1.22	2.70e-03
hsa-miR-142-3p		-0.98	-1*	2.60e-03
hsa-miR-150-5p		1.08	1.1	2.70e-03
hsa-miR-29c-3p		-3.98	-4.01	9.70e-06
hsa-miR-486-5p		3.21	3.34*	8.10e-06

C

Mixed 4-tissue Cardiac Tissue miRNA (Doxorubicin vs Control)				
miRNA	GSEA plot	NES	FC	pval
hsa-miR-143-3p		511.1	521.12	9.10e-31
hsa-miR-199a-5p		291.1	310.12	8.10e-26
hsa-miR-107-5p		3.25	3.32	9.70e-06
hsa-miR-320a		3.45	3.52	9.80e-06
hsa-miR-103a-3p		3.82	3.91	9.90e-06
hsa-miR-145-5p		561.2	581.21	8.10e-34
hsa-miR-181a-5p		18.23	18.43	4.50e-19
hsa-miR-100-5p		723.1	750.21	5.60e-41
hsa-miR-499a-5p		0.99	1.01*	1.00e-03
hsa-miR-146a-5p		1.92	1.98	2.80e-04
hsa-miR-210-3p		11.82	11.91	4.10e-15
hsa-miR-92a-3p		1.98	2.01*	1.20e-04
hsa-miR-342-3p		1.34	1.43	3.10e-03
hsa-miR-142-3p		-1.18	-1.21*	2.10e-03
hsa-miR-150-5p		0.97	0.99	1.02e-02
hsa-miR-29c-3p		-1.12	-1.15	1.10e-03
hsa-miR-486-5p		1.01	1.04*	1.00e-03

Supplementary Figure 12 | *In vitro* biomarkers of doxorubicin cardiomyopathy in perfusate of multi-tissue chips. a, Schematic detailing workflow characterizing miRNA expression between perfusate sampled from the recirculating media of the 4-Tissue *Multi-organ* and *Mixed* tissue chips after doxorubicin treatment. **b-c,** Gene set enrichment analysis (GSEA) of miRNAs from perfusate of the 4-Tissue *Multi-organ* (**b**) and 4-Tissue *Mixed* (**c**) tissue chips after doxorubicin treatment as benchmarked against clinically identified biomarkers of doxorubicin toxicity in a pediatric study (Oatmen et al., 2018). (*Consistent with clinical finding; Color codes – Blue (Negative Fold-Change), Red (Positive Fold-Change))

Tissue	Tissue schematic	ECM	Cell type	Seeding density per tissue	Total number of cells	Dimensions	Total tissue volume
Liver	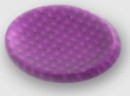	Fibrin	hiPSC-derived hepatocytes and NHDF	$5x10^5$ cells of each type	$1x10^6$	9 mm x 2.1 mm (diameter x height)	134 mm^3
Heart	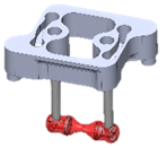	Fibrin	hiPSC-derived cardiomyocytes and NHDF	$7.5x10^5$ of cardiomyocytes and $2.5x10^5$ of NHDF	$1x10^6$	6.4 mm x 2.3 mm x 2 mm (length x width x height)	30 mm^3
Bone		Deccelularized bone scaffold	MSC-derived osteoblasts and primary monocytes-derived osteoclasts	$4x10^5$ cells of each cell	$8x10^5$	8 mm x 4 mm x 1 mm (length x width x height)	32 mm^3
Skin	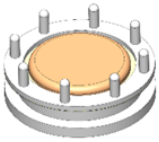	Collagen I	NHDF and keratinocytes	$1.5x10^5$ of NHDF and $2.5 x10^5$ of keratinocytes	$4x10^5$	6.8 mm x 2.5 mm (diameter x height)	91 mm^3
Endothelial barrier		Fibronectin	HUVEC and MSC	$1.5x10^5$ of MSC in the apical side, and $4x10^5$ of HUVEC and $5x10^4$ of MSC in the basal side	$6x10^5$	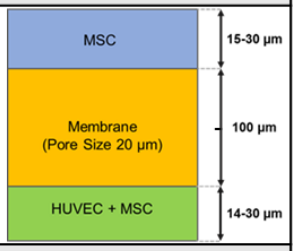	
Monocytes		-	Primary $CD14^+$ monocytes	$5x10^4$ cells	$5x10^4$	-	-

Supplementary Table 1 | Tissue specifications. Extracellular matrix (ECM), cell types and numbers, dimensions, and volume for each tissue. hiPSC, human induced pluripotent stem cell; NHDF, normal human dermal fibroblasts; MSC, mesenchymal stem cell; HUVEC, human umbilical endothelial cell.

Circulating Endothelial Media:	Cardiac Tissue Media:	Bone Tissue Media:
Endothelial Basal Media (EBM)	**RPMI**	**EMEM Basal Media**
EGM-2 Media Supplement:	Penicillin/Streptomycin	FBS
Fetal Bovine Serum (FBS)	**B27 Supplement:**	Penicillin/Streptomycin
Hydrocortisone	Biotin	M-CSF
Human basic fibroblast growth factor (hFGF-B)	DL alpha tocopherol acetate	sRANKL
Vascular endothelial growth factor (VEGF)	DL alpha-tocopherol	
Long Arg3 insulin-like growth factor-1 (R3-IGF-1)	Vitamin A (acetate)	
Ascorbic Acid	Bovine serum albumin (BSA, fatty acid free fraction V)	**Skin Tissue Media:**
Human epidermal growth factor (hEGF)	Catalase	**DMEM/F12**
Gentamicin sulfate-amphotericin (GA-1000)	Human recombinant insulin	Adenine
Heparin	Human transferrin	Hydrocortisone
	Superoxide dismutase	T3 (triodo-l-thyronine)
	Corticosterone	Insulin-transferrin-selenium (ITS)
Liver Tissue Media:	D-galactose	Ascorbic acid
Hepatic Basal Media (HCM)	Ethanolamine HCl	Ethanolamine and phosphorylethanolamine (EOP)
HCM Media Supplement:	Glutathione (reduced)	Calcium chloride
Transferrin	L-carnitine HCl	FBS
Ascorbic acid	Linoleic acid	Penicillin/Streptomycin
Insulin	Linolenic acid	
Hydrocortisone	Progesterone	
BSA (fatty-acid free)	Putrescine 2HCl	
GA-1000	Sodium selenite	
	T3 (triodo-l-thyronine)	

Supplementary Table 2 | Media compositions for each tissue type. Each tissue compartment contained 1.5 mL of media (liver, heart, bone, or skin) and the vascular compartment contained 12 mL of endothelial media.

Modeling parameters		
Parameter	**Value**	**Reference**
V_{max}	350 pmol $(mg.min)^{-1}$	(Kassner et al., 2008)
K_m	170 µM	(Kassner et al., 2008)
f_u	1	(Sakolish et al., 2020)
LogP	1.27	(Wishart et al., 2008)
$S_{L,el}$	43.5 L h^{-1}	(Gustafson et al., 2002)
Q_{cl}	0.5×10^{-10} m^3 s^{-1}	Calibrated
D_1	2.12×10^{-10} m^2 s^{-1}	(Biondi et al., 2013)
D_2	1.58×10^{-11} m^2 s^{-1}	(Qian et al., 2003)

Supplementary Table 3 | Modeling parameters. V_{max}, maximum reaction rate; K_m, Michaelis constant; F_u, unbound fraction of the drug LogP, lipophilicity; $S_{L,el}$, compound elimination rate; Q_{cl}, clearance flow rate; D_1, diffusivity of the drug in the compartments containing media; D_2, diffusivity of the drug in the solid compartments.

Extended Data Fig. 9A	
Variable	**Meaning**
S	Skin
ST	Skin tank
B	Bone
BT	Bone tank
H	Heart
HT	Heart tank
L	Liver
LT	Liver tank
Q_f	Flow rate
LIFC	Liver inlet fluidic channel
LFC	Liver fluidic channel
HIFC	Heart inlet fluidic channel
HFC	Heart fluidic channel
BIFC	Bone inlet fluidic channel
BFC	Bone fluidic channel
SIFC	Skin inlet fluidic channel
SFC	Skin fluidic channel
SOFC	Skin outlet fluidic channel
SMM	Endothelial membrane below the skin tank
BMM	Endothelial membrane below the bone tank
HMM	Endothelial membrane below the heart tank
LMM	Endothelial membrane below the liver tank
Extended Data Fig. 9B	
Variable	**Meaning**
J	Flux between two different compartments or tissue
V	Volume of compartment or tissue
C	Concentration of a compound in a compartment or tissue
LTT	Top layer of the liver tank
LMT	Middle layer of the liver tank
LBT	Bottom layer of the liver tank
LTM	Top layer of the endothelial barrier below the liver tank
LMM	Middle layer of the endothelial barrier below the liver tank
LBM	Bottom layer of the endothelial barrier below the liver tank
LFC	Liver fluidic channel
LIFC	Liver inlet fluidic channel
TB20	Section 20 of the tubing lumen
L	Liver tissue
Q_f	Flow rate
$J_{LMT-LTT}$	Flux between the middle and the top layers of the liver tank
$J_{LBT-LMT}$	Flux between the bottom and the middle layers of the liver tank
$J_{LTM-LBT}$	Flux between the top layer of the endothelial barrier below the liver tank and the bottom layer of the liver tank
J_{LBT-L}	Flux between the bottom layer of the liver tank and the liver tissue
$J_{LMM-LTM}$	Flux between the middle and the top layers of the endothelial barrier below the liver tank
$J_{LBM-LMM}$	Flux between the bottom and the middle layers of the endothelial barrier below the liver tank
$J_{LFC-LBM}$	Flux between the liver fluidic channel and the bottom layer of the endothelial barrier below the liver tank

V_{LTT}	Volume of the top layer of the liver tank
C_{LTT}	Concentration of the top layer of the liver tank
V_{LMT}	Volume of the middle layer of the liver tank
C_{LMT}	Concentration in the middle layer of the liver tank
V_{LBT}	Volume of the bottom layer of the liver tank
C_{LBT}	Concentration in bottom layer of the liver tank
V_L	Volume of liver tissue
C_L	Concentration in the liver tissue
V_{LTM}	Volume of the top layer of the endothelial barrier below the liver tank
C_{LTM}	Concentration in the top layer of the endothelial barrier below the liver tank
V_{LMM}	Volume of middle layer of the endothelial barrier below the liver tank
C_{LMM}	Concentration in the middle layer of the endothelial barrier below the liver tank
V_{LBM}	Volume of bottom layer of the endothelial barrier below the liver tank
C_{LBM}	Concentration in the bottom layer of the endothelial barrier below the liver tank
V_{LFC}	Volume of the liver fluidic channel
C_{LFC}	Concentration in the liver fluidic channel
V_{LIFC}	Volume of the liver inlet fluidic channel
C_{LIFC}	Concentration in the liver inlet fluidic channel
C_{TB20}	Concentration in section 20 of the tubing lumen
Extended Data Fig. 9C	
Variable	**Meaning**
J	Flux between two different compartments or tissue
V	Volume of compartment or tissue
C	Concentration of a compound in a compartment or tissue
HTT	Top layer of the heart tank
HMT	Middle layer of the heart tank
HBT	Bottom layer of the heart tank
HTM	Top layer of the endothelial barrier below the heart tank
HMM	Middle layer of the endothelial barrier below the heart tank
HBM	Bottom layer of the endothelial barrier below the heart tank
HFC	Heart fluidic channel
HIFC	Heart inlet fluidic channel
LFC	Liver fluidic channel
H	Heart tissue
Q_f	Flow rate
J_{HTT-PD}	Flux between the top layer of the heart tank and the PDMS pillars
$J_{HMT-HTT}$	Flux between the middle and the top layers of the heart tank
J_{HMT-PD}	Flux between the middle layer of the heart tank and the PDMS pillars
$J_{HBT-HMT}$	Flux between the bottom and the middle layers of the heart tank
J_{HMT-H}	Flux between the middle layer of the heart tank and the heart tissue
$J_{HTM-HBT}$	Flux between the top layer of the endothelial barrier below the heart tank and the bottom layer of the heart tank
$J_{HMM-HTM}$	Flux between the middle and the top layers of the endothelial barrier below the heart tank
$J_{HBM-HMM}$	Flux between the bottom and the middle layers of the endothelial barrier below the hear tank
$J_{HFC-HBM}$	Flux between the heart fluidic channel and the bottom layer of the endothelial barrier below the heart tank
V_{HTT}	Volume of the top layer of the heart tank
C_{HTT}	Concentration in the top layer of the heart tank
V_{HMT}	Volume of the middle layer of the heart tank
C_{HMT}	Concentration in the middle layer of the heart tank
V_{HBT}	Volume of the bottom layer of the heart tank
C_{HBT}	Concentration in the bottom layer of the heart tank
V_H	Volume of the heart tissue

C_H	Concentration in the heart tissue
V_{HTM}	Volume of the top layer of the endothelial barrier below the heart tank
C_{HTM}	Concentration in the top layer of the endothelial barrier below the heart tank
V_{HMM}	Volume of the middle layer of the endothelial barrier below the heart tank
C_{HMM}	Concentration in the middle layer of the endothelial barrier below the heart tank
V_{HBM}	Volume of the bottom layer of the endothelial barrier below the heart tank
C_{HBM}	Concentration in the bottom layer of the endothelial barrier below the heart tank
V_{HFC}	Volume of the heart fluidic channel
C_{HFC}	Concentration in the heart fluidic channel
V_{HIFC}	Volume of the heart inlet fluidic channel
C_{HIFC}	Concentration in the heart inlet fluidic channel
C_{LFC}	Concentration in the liver fluidic channel
Extended Data Fig. 9D	
Variable	**Meaning**
J	Flux between two different compartments or tissue
V	Volume of compartment or tissue
C	Concentration of a compound in a compartment or tissue
B	Bone tissue
BTT	Top layer of the bone tank
BMT	Middle layer of the bone tank
BBT	Bottom layer of the bone tank
BTM	Top layer of the endothelial barrier below the bone tank
BMM	Middle layer of the endothelial barrier below the bone tank
BBM	Bottom layer of the endothelial barrier below the bone tank
BFC	Bone fluidic channel
BIFC	Bone inlet fluidic channel
HFC	Heart fluidic channel
Q_f	Flow rate
$J_{BMT-BTT}$	Flux between the middle and the top layers of the bone tank
$J_{BBT-BMT}$	Flux between the bottom and the middle layers of the bone tank
J_{BBT-B}	Flux between the bottom layer of the bone tank and the bone tissue
J_{BTM-B}	Flux between the top layer of the endothelial barrier below the bone tank and the bone tissue
$J_{BMM-BTM}$	Flux between the middle and the top layers of the endothelial barrier below the bone tank
$J_{BBM-BMM}$	Flux between the bottom and the middle layers of the endothelial barrier below the bone tank
$J_{BFC-BBM}$	Flux between the bone fluidic channel and the bottom layer of the endothelial barrier below the bone tank
V_{BTT}	Volume of the top layer of the bone tank
C_{BTT}	Concentration in the top layer of the bone tank
V_{BMT}	Volume of the middle layer of the bone tank
C_{BMT}	Concentration in the middle layer of the bone tank
V_{BBT}	Volume of the bottom layer of the bone tank
C_{BBT}	Concentration in the bottom layer of the bone tank
V_B	Volume of the bone tissue
C_B	Concentration in the bone tissue
V_{BTM}	Volume of the top layer of the endothelial barrier below the bone tank
C_{BTM}	Concentration in the top layer of the endothelial barrier below the bone tank
V_{BMM}	Volume of middle layer of the endothelial barrier below the bone tank
C_{BMM}	Concentration in the middle layer of the endothelial barrier below the bone tank
V_{BBM}	Volume of bottom layer of the endothelial barrier below the bone tank
C_{BBM}	Concentration in the bottom layer of the endothelial barrier below the bone tank
V_{BFC}	Volume of the bone fluidic channel
C_{BFC}	Concentration in the bone fluidic channel

V_{BIFC}	Volume of the bone inlet fluidic channel
C_{BIFC}	Concentration in the bone inlet fluidic channel
C_{HFC}	Concentration in heart fluidic channel
Extended Data Fig. 9E	
Variable	**Meaning**
J	Flux between two different compartments or tissue
V	Volume of compartment or tissue
C	Concentration of a compound in a compartment or tissue
S	Skin tissue
STT	Top layer of the skin tank
SMT	Middle layer of the skin tank
SBT	Bottom layer of the skin tank
STM	Top layer of the endothelial barrier below the skin tank
SMM	Middle layer of the endothelial barrier below the skin tank
SBM	Bottom layer of the endothelial barrier below the skin tank
SOFC	Skin outlet fluidic channel
SFC	Skin fluidic channel
SIFC	Skin inlet fluidic channel
BFC	Bone fluidic channel
Q_f	Flow rate
J_{STT-S}	Flux between the top layer of the skin tank and the skin tissue
$J_{SMT-STT}$	Flux between the middle and the top layers of the skin tank
$J_{SBT-SMT}$	Flux between the bottom and the middle layers of the skin tank
$J_{STM-SBT}$	Flux between the top layer of the endothelial barrier below the skin tank and the bottom layer of the skin tank
$J_{SMM-STM}$	Flux between the middle and the top layers of the endothelial barrier below the skin tank
$J_{SBM-SMM}$	Flux between the bottom and the middle layers of the endothelial barrier below the skin tank
$J_{SFC-SBM}$	Flux between the skin fluidic channel and the bottom layer of the endothelial barrier below the skin tank
V_{STT}	Volume of the top layer of the skin tank
C_{STT}	Concentration in the top layer of the skin tank
V_{SMT}	Volume of the middle layer of the skin tank
C_{SMT}	Concentration in the middle layer of the skin tank
V_{SBT}	Volume of the bottom layer of the skin tank
C_{SBT}	Concentration in the bottom layer of the skin tank
V_S	Volume of the skin tissue
C_S	Concentration in the skin tissue
V_{STM}	Volume of the top layer of the endothelial barrier below the skin tank
C_{STM}	Concentration in the top layer of the endothelial barrier below the skin tank
V_{SMM}	Volume of middle layer of the endothelial barrier below the skin tank
C_{SMM}	Concentration in the middle layer of the endothelial barrier below the skin tank
V_{SBM}	Volume of bottom layer of the endothelial barrier below the skin tank
C_{SBM}	Concentration in the bottom layer of the endothelial barrier below the skin tank
V_{SOFC}	Volume of the skin outlet fluidic channel
C_{SOFC}	Concentration in the skin outlet fluidic channel
V_{SFC}	Volume of the skin fluidic channel
C_{SFC}	Concentration in the skin fluidic channel
V_{SIFC}	Volume of the skin inlet fluidic channel
C_{SIFC}	Concentration in the skin inlet fluidic channel
C_{BFC}	Concentration in the bone fluidic channel
Extended Data Fig. 9F	
Variable	**Meaning**
J	Flux between two different compartments or tissue

V	Volume of compartment or tissue
C	Concentration of a compound in a compartment or tissue
RES	Reservoir
i	Section i of the tubing wall or lumen (i = 2 - 19)
TB,1	Section 1 of the tubing wall
TB,2	Section 2 of the tubing wall
TB,i-1	Section i-1 of the tubing wall
TB,i	Section i of the tubing wall
TB,i+1	Section i+1 of the tubing wall
TB,19	Section 19 of the tubing wall
TB,20	Section 20 of the tubing wall
TL,1	Section 1 of the tubing lumen
TL,2	Section 2 of the tubing lumen
TL,i-1	Section i-1 of the tubing lumen
TL,i	Section i of the tubing lumen
TL,i+1	Section i+1 of the tubing lumen
TL,19	Section 19 of the tubing lumen
TL,20	Section 20 of the tubing lumen
SOFC	Skin outlet fluidic channel
Q_f	Flow rate
$J_{TL,1-TB,1}$	Flux between sections 1 of the tubing lumen and wall
$J_{TB,1-TB,2}$	Flux between sections 1 and 2 of the tubing wall
$J_{TL,1-TL,2}$	Flux between sections 1 and 2 of the tubing lumen
$J_{TB,i-1-TB,i}$	Flux between sections i-1 and i of the tubing wall
$J_{TL,i-1-TL,i}$	Flux between sections i-1 and i of the tubing lumen
$J_{TL,i-TB,i}$	Flux between sections i of the tubing lumen and wall
$J_{TB,i-TB,i+1}$	Flux between sections i and i+1 of the tubing wall
$J_{TL,i-TL,i+1}$	Flux between sections i and i+1 of the tubing lumen
$J_{TB,19-TB,20}$	Flux between sections 19 and 20 of the tubing wall
$J_{TL,19-TL,20}$	Flux between sections 19 and 20 of the tubing lumen
$J_{TL,20-TB,20}$	Flux between sections 20 of the tubing lumen and wall
C_{SOFC}	Concentration in the skin outlet fluidic channel
V_{RES}	Volume in the reservoir
C_{RES}	Concentration in the reservoir
$V_{TB,1}$	Volume in section 1 of the tubing wall
$C_{TB,1}$	Concentration in section 1 of the tubing wall
$V_{TL,1}$	Volume in section 1 of the tubing lumen
$C_{TL,1}$	Concentration in section 1 of the tubing lumen
$V_{TB,i}$	Volume in section i of the tubing wall
$C_{TB,i}$	Concentration in section i of the tubing wall
$V_{TL,i}$	Volume in the section i of the tubing lumen
$C_{TL,i}$	Concentration in section i of the tubing lumen
$V_{TB,20}$	Volume in the section 20 of the tubing wall
$C_{TB,20}$	Concentration in section 20 of the tubing wall
$V_{TL,20}$	Volume in the section 20 of the tubing lumen
$C_{TL,20}$	Concentration in section 20 of the tubing lumen
Supplementary Fig. 6	
Variable	**Meaning**
J	Flux between two different compartments or tissue
V	Volume of compartment or tissue
C	Concentration of a compound in a compartment or tissue
BT	Bottom layer of the tank
MM	Membrane below the tank

FC	Fluidic channel below the membrane
B	Bone tissue
BMM	Membrane below the bone tank
BFC	Bone fluidic channel
Q_f	Flow rate
J_{MM-BT}	Flux between the membrane below the tank and the bottom layer of the tank
J_{FC-MM}	Flux between the fluidic channel below the membrane and the membrane bellow the tank
J_{BMM-B}	Flux between the membrane below the bone tank
$J_{BFC-BMM}$	Flux between the bone fluidic channel and the membrane below the bone tank
V_{BT}	Volume of the bottom layer of the tank
C_{BT}	Concentration in the bottom layer of the tank
V_{MM}	Volume of the membrane below the tank
C_{MM}	Concentration in the membrane below the tank
V_{FC}	Volume of the fluidic channel below the membrane
C_{FC}	Concentration in the fluidic channel below the membrane
V_B	Volume of the bone tissue
C_B	Concentration in bone tissue
V_{BMM}	Volume of the membrane below the bone tank
C_{BMM}	Concentration in membrane below the bone tank
V_{BFC}	Volume of the bone fluidic channel
C_{BFC}	Concentration in the bone fluidic channel

Supplementary Table 4 | Terms used in the computational model and their meaning.

Supplementary Video 1 | Assembly of the tissue chip.

Supplementary References

Biondi, M., Fusco, S., Lewis, A. L., & Netti, P. A. (2013). Investigation of the mechanisms governing doxorubicin and irinotecan release from drug-eluting beads: Mathematical modeling and experimental verification. *Journal of Materials Science: Materials in Medicine*, *24*(10), 2359–2370. https://doi.org/10.1007/s10856-013-4992-4

Gustafson, D. L., Rastatter, J. C., Colombo, T., & Long, M. E. (2002). Doxorubicin pharmacokinetics: Macromolecule binding, metabolism, and excretion in the context of a physiologic model. *Journal of Pharmaceutical Sciences*, *91*(6), 1488–1501. https://doi.org/10.1002/jps.10161

Kassner, N., Huse, K., Martin, H.-J., Gödtel-Armbrust, U., Metzger, A., Meineke, I., Brockmöller, J., Klein, K., Zanger, U. M., Maser, E., & Wojnowski, L. (2008). Carbonyl reductase 1 is a predominant doxorubicin reductase in the human liver. *Drug Metabolism and Disposition*, *36*(10), 2113–2120. https://doi.org/10.1124/dmd.108.022251

Oatmen, K.E., Toro-Salazar, O.H., Hauser, K., Zellars, K.N., Mason, K.C., Hor, K., Gillan, E., Zeiss, C.J., Gatti, D.M., & Spinale, F.G. (2018). Identification of a novel microRNA profile in pediatric patients with cancer treated with anthracycline chemotherapy. *American Journal of Physiology. Heart and Circulatory Physiology, 315*(5), H1443-H1452. doi: 10.1152/ajpheart.00252.2018.

Qian, F., Stowe, N., Liu, E. H., Saidel, G. M., & Gao, J. (2003). Quantification of in vivo doxorubicin transport from PLGA millirods in thermoablated rat livers. *Journal of Controlled Release*, *91*(1–2), 157–166. https://doi.org/10.1016/s0168-3659(03)00237-2

Sakolish, C., House, J. S., Chramiec, A., Liu, Y., Chen, Z., Halligan, S. P., Vunjak-Novakovic, G., & Rusyn, I. (2020). Tissue-engineered bone tumor as a reproducible human in vitro model for studies of anticancer drugs. *Toxicological Sciences*, *173*(1), 65–76. https://doi.org/10.1093/toxsci/kfz220

Wishart, D. S., Knox, C., Guo, A. C., Cheng, D., Shrivastava, S., Tzur, D., Gautam, B., & Hassanali, M. (2008). DrugBank: A knowledgebase for drugs, drug actions and drug targets. *Nucleic Acids Research*, *36*(Database issue), D901-906. https://doi.org/10.1093/nar/gkm958

Yadi, W., Shurui, C., Tong, Z., Suxian, C., Qing, T., & Dongning, H. (2020). Bioinformatic analysis of peripheral blood miRNA of breast cancer patients in relation with anthracycline cardiotoxicity. *BMC Cardiovascular Disorders*, *20*(1), 43. doi: 10.1186/s12872-020-01346-y.